Generalized multi-terminal decoherent transport: Recursive algorithms and applications to SASER and giant magnetoresistance.

Carlos J. Cattena[1] Lucas J. Fernández-Alcázar[1], Raúl A.
Bustos-Marún[1,2], Daijiro Nozaki[3] and Horacio M. Pastawski[1]

Decoherent transport in mesoscopic and nanoscopic systems can be formulated in terms of the
D'Amato-Pastawski (DP) model. This generalizes the Landauer-Büttiker picture by considering
a distribution of local decoherent processes. However, its generalization for multi-terminal setups
is lacking. We first review the original two-terminal DP model for decoherent transport. Then,
we extend it to a matrix formulation capable of dealing with multi-terminal problems. We also
introduce recursive algorithms to evaluate the Green's functions for general banded Hamiltonians as
well as local density of states, effective conductances and voltage profiles. We finally illustrate the
method by analyzing two problems of current relevance. 1) Assessing the role of decoherence in a
model for phonon lasers (SASER). 2) Obtaining the classical limit of Giant Magnetoresistance from
a spin-dependent Hamiltonian. The presented methods should pave the way for computationally
demanding calculations of transport through nanodevices, bridging the gap between fully coherent
quantum schemes and semiclassical ones.

PACS numbers: 73.23.-b, 73.63.-b, 71.15.Dx, 72.10.Di

I. INTRODUCTION

Quantum transport at the nanoscale [1–3] is a blooming field where the properties of matter can be explored in a realm where quantum effects become crucial. In particular, the control of quantum interference phenomena and their interplay with the electronic structure offers a fascinating opportunity to overcome some of the usual constraints of our macroscopic classical world. [4–8] However, at the nanoscale, both quantum *and* classical behavior can be expected. This last emerges from the unavoidable environmental degrees of freedom. [9] An exciting example of the competition among those behaviors is electron-transfer in natural and artificial photosynthesis. There, the interplay between localizing interferences and environmentally induced decoherence seems to have a fundamental role in optimizing excitonic transfer. [10, 11] This phenomenon falls in line with what is known in low dimensional conductors. Indeed, transport properties of highly ordered 1-D systems is determined by the fast quantum diffusion of local excitations, and thus become weakened by decoherence. On the other hand, in disordered 1-D wires, quantum coherence allows the destructive interferences that produce electronic localization. While these phenomena are roughly described by introducing imaginary energies in the Kubo formulation, it is at the cost of overlooking charge conservation. [12]

Landauer's picture has almost no rival in what concerns to electronic coherent transport.[13] In its simplest form, conductance is determined by the transmission probability (either quantum or classical) among electrodes. Paradoxically, quantum transmittance is much simpler to evaluate than its classical counterpart. Thus, the great majority of work focus on the evaluation of the coherent transmittance setting aside incoherent processes. An extension of this approach, developed by Markus Büttiker,[14] applies the Kirchhoff laws to a system connected to multiple terminals. This allows to consider different voltage probes as well as multiple current sources and drains. The self-consistent non-equilibrium chemical potentials at the voltmeters must ensure current cancellation. The resulting transport coefficients fulfill the Onsager's reciprocity relations. Additionally, Büttiker had the crucial insight[15] that a voltage probe implies a classical measurement and thus it acts as a decoherence source. This concept was further formulated by D'Amato and Pastawski introducing a Hamiltonian description [16] (henceforth the DP model). In this description, the decoherent local probes can be assimilated to incoherent scattering by delta-function potentials[17, 18]. This is founded in the Keldysh, Kadanoff and Baym's quantum fields formalism[19] for the non-equilibrium Green's functions. [19–21] There, the integro-differential equations are simplified by evaluating the currents and chemical potentials in a linearized scheme that involves a matrix containing only transmittances among different points in the sample. The DP model also provides a compact solution for an arbitrary distribution of incoherent local scattering processes. These lead to a momentum relaxing decoherence that produces diffusion and a further increase in the resistance. The final set of linear equations relate the local chemical potentials and the currents through a transmittances matrix. [22] This results in the Generalized Landauer-Büttiker Equations (GLBE) that solve the DP model.

The original presentation of the DP model is constrained to two terminal problems. Thus, in spite of the growing need to include the effects of decoherent processes,[23, 24] its applications remained mostly reduced to a few one-dimensional problems. [25–31] Besides, since the method deals with a great number of self-consistent local chemical potentials, it often involves a cumbersome matrix inversion. Thus, a general multi-terminal formulation of the DP model for decoherent transport and an efficient computational strategy are still

lacking.

In this paper we generalize the D'Amato-Pastawski model for multi-terminal problems, presenting a decimation-based method for the calculation of the decoherent conductance. In Sec. II we introduce the basic tools, based on a decimation procedure that yields the parameters of an effective Hamiltonian. In Sec. III we overview the original DP model. In Sec. IV, we generalize the DP model for multi-terminal setups. We also provide a recursive algorithm for the calculation of Green's functions of general banded Hamiltonians. Then, we show two application examples. In Sec. V we consider a simple model of a phonon-laser (SASER) based on the electron-phonon interaction in a quantum dot [32] where we asses the role of decoherence in the SASER efficiency. In Sec. VI, we consider the spin dependent electronic transport in a ferromagnetic wire where the Giant Magnetoresistance (GMR) [33] shows up. We show that our formulation describes the complete cross-over from a quantum transport to the GMR semiclassical regime. In Sec. VII we summarize our results and conclude that our formulation can handle decoherent transport in a wide variety of problems beyond the typical two-terminal calculations.

II. DECIMATION PROCEDURES AND EFFECTIVE HAMILTONIANS

Even the simplest quantum devices involve a huge number of degrees of freedom and thus their study can not be carried out without proper simplifications. For example, a tight-binding Hamiltonian describing a device or molecule with N states (or orbitals) is, [34]

$$\hat{H}_S = \sum_{i=1}^{N} \left\{ E_i \hat{c}_i^\dagger \hat{c}_i + \sum_{\substack{j=1 \\ (j \neq i)}}^{N} \left[V_{i,j} \hat{c}_i^\dagger \hat{c}_j + V_{j,i} \hat{c}_j^\dagger \hat{c}_i \right] \right\}. \quad (1)$$

Here, $\hat{c}_i^\dagger$ and $\hat{c}_i$ correspond to the creation and anihilation fermionic operators acting on the vacuum $|0\rangle$. Site energies are E_i and hopping amplitudes $V_{i,j}$ define the matrix Hamiltonian whose single particle eigenstates are $|k\rangle = \sum_i u_{i,k} \hat{c}_i^\dagger |0\rangle$ of energy ε_k which are filled up to the Fermi energy, ε_F.

The decimation procedures, inspired in the renormalization group techniques of statistical mechanics [35, 36], seek to recursively reduce the number of degrees of freedom of a general $N \times N$ Hamiltonian into another of lower rank, without altering the physical properties. The basic idea can be captured by considering a system with $N = 3$ states whose secular equation is:

$$\begin{bmatrix} \varepsilon - E_1 & -V_{12} & -V_{13} \\ -V_{21} & \varepsilon - E_2 & -V_{23} \\ -V_{31} & -V_{32} & \varepsilon - E_3 \end{bmatrix} \begin{pmatrix} u_1 \\ u_2 \\ u_3 \end{pmatrix} = [\varepsilon \mathbb{I} - \mathbb{H}_S] \vec{u} \equiv \vec{0}. \quad (2)$$

Quite often we are interested in the transfer of an excitation from an initial state to another one, say 1 and 2. Thus, instead of diagonalizing the matrix, we could isolate u_3 from the third row and use it to eliminate u_3 in the first and the second equations. In this way, we obtain a new set of equations where u_3 is *decimated*:

$$\begin{bmatrix} \varepsilon - \overline{E}_1 & -\overline{V}_{12} \\ -\overline{V}_{21} & \varepsilon - \overline{E}_2 \end{bmatrix} \begin{pmatrix} u_1 \\ u_2 \end{pmatrix} = [\varepsilon \mathbb{I} - \mathbb{H}_{\text{eff.}}] \vec{u} = 0. \quad (3)$$

The renormalized coefficients hide their non-linear dependence on the energy variable ε :

$$\overline{E}_1 = E_1 + \Sigma_1(\varepsilon) = E_1 + V_{13} \frac{1}{\varepsilon - E_3} V_{31},$$
$$\overline{E}_2 = E_2 + \Sigma_2(\varepsilon) = E_2 + V_{23} \frac{1}{\varepsilon - E_3} V_{32}, \quad (4)$$
$$\overline{V}_{12} = V_{12} + V_{13} \frac{1}{\varepsilon - E_3} V_{32}.$$

In this case, the terms $\Sigma_j(\varepsilon); j = 1, 2$ are the real self-energies accounting for the energy shifts due to the coupling with the eliminated state. Notice that as long as one conserves the analytical dependence on ε of Σ_j, the actual secular equation is still cubic in ε and provides the exact spectrum of the whole system. This procedure can be performed systematically in a Hamiltonian of any size $N \times N$ to end up with an effective Hamiltonian of size one desires, in particular a 2×2 one. The effective interaction parameter $\overline{V}_{12}$, together with the self-energies Σ_j, accounts for transport through the whole sample. Their dependence on ε provides all the needed information on the steady state transport as well as on quantum dynamics. [37] In practice, it is convenient to add an infinitesimal imaginary part, $-i\eta$, to each energy $E_j \to E_j - i\eta$. Since a finite $\eta > 0$ is equivalent to a decay process, it ensures that one recovers the retarded time dependences of the observables through a well defined Fourier transform.

The terminals connected to the system are described as semi-infinite leads coupled to it. They are handled in a similar way as the system itself. The idea is to eliminate all the internal degrees of freedom decimating them progressively, renormalizing the states of the system which are directly coupled to the external reservoirs. For further clarification we consider a lead modeled as a semi-infinite one dimensional chain,

$$\hat{H}_L = \sum_{i=0}^{-\infty} \left\{ E_i \hat{c}_i^\dagger \hat{c}_i - V \left[\hat{c}_i^\dagger \hat{c}_{i-1} + \hat{c}_{i-1}^\dagger \hat{c}_i \right] \right\}, \quad (5)$$

that yields a tridiagonal matrix of infinite dimension. The elements E_i's and V's are now the diagonal and off-diagonal terms of a tridiagonal matrix $\mathbb{H}_L$. This lead is connected at the left of the system, say, with site 1:

$$\hat{V}_{SL} = V_L \left[\hat{c}_1^\dagger \hat{c}_0 + \hat{c}_0^\dagger \hat{c}_1 \right]. \quad (6)$$

Instead of dealing with the whole Hamiltonian

$$\hat{H} = \hat{H}_S + \hat{H}_L + \hat{V}_{SL}, \quad (7)$$

we perform the decimation procedure. It becomes particularly simple because of the chain structure of the lead. The energy of the i-th site, is "shifted" by the elimination of $(i-1)$-th site, which itself is shifted by sites at its left [34], with the self-energies resulting in a continued-fraction:

$$\Sigma_i = V_{i,i-1} \frac{1}{\varepsilon - E_{i-1} - \Sigma_{i-1}} V_{i-1,i} \qquad (8)$$
$$(i = 0, -1, -2, \dots - \infty)$$

In a perfect propagating channel: $V_{i,i-1} \equiv V$ and $E_i = E_0$, and thus, $\Sigma_i = \Sigma_{i-1} \equiv \Sigma$, we arrive to the self-consistent solution:

$$\Sigma(\varepsilon) = \frac{V^2}{\varepsilon - E_0 - \Sigma} = \Delta(\varepsilon) - i\Gamma(\varepsilon).$$
$$= \frac{\varepsilon - E_0 + i\eta}{2} - \mathrm{sgn}(\varepsilon - E_0)\sqrt{\left(\frac{\varepsilon - E_0 + i\eta}{2}\right)^2 - V^2} \quad (9)$$

where the generalized square root [38] in the limit $\eta \to 0^+$, yields the imaginary component of the self-energy for ε within the band of allowed energies. It becomes real otherwise.

Thus, once the states in the left lead are fully decimated the energy of the first site becomes

$$\widetilde{E}_1(\varepsilon) = \overline{E}_1(\varepsilon) + \Sigma_{L1}(\varepsilon) \qquad (10)$$

$$\text{with} \quad \Sigma_{L1}(\varepsilon) = \left(\frac{V_L}{V}\right)^2 \Sigma(\varepsilon) \qquad (11)$$

$$= \Delta_{L1}(\varepsilon) - i\Gamma_{L1}(\varepsilon) \qquad (12)$$

As before, the real part $\Delta_{L1}(\varepsilon)$ indicates how the unperturbed site energies are shifted by the leads. The important difference with the simple decimation example discussed above is that, as a consequence of the infinite nature of the lead, the self-energies may acquire a finite imaginary component, $\Gamma_{L1}(\varepsilon)$, even in the limit $\eta \to 0^+$. It describes the rate at which coherent density excitation in the system decays into the lead propagating states.

Note that, the imaginary part is roughly consistent with the exponential decays of the survival probability predicted by the Fermi Golden Rule (FGR). For instance, in a "system" with a single state $|1\rangle$ interacting with a lead, the survival probability at time t after it has been placed in state $|1\rangle$ is,

$$\left| \langle 1| \exp[-i\hat{H}\ t/\hbar] |1\rangle\ \theta(t) \right|^2 \equiv \left| i\hbar G_{11}^R(t) \right|^2 \qquad (13)$$
$$\simeq \exp[-2\Gamma_{L1}(E_1)t/\hbar] \qquad (14)$$

where we introduced the time dependent retarded Green's function, $G_{11}^R(t)$. However, we remember that the self-energies obtained above have an explicit functional dependence on ε. In consequence, the actual decay can depart from this naive exponential approximation. Indeed, a quantum decay should start quadratically as $1 - (V_L t/\hbar)^2$ turning into an exponential at very short times. At very long times the decay may even become

a non-monotonous. [39] In practice, we will stay in the exponential approximation by neglecting the dependence on ε unless it is close to a band edge.

For the sake of simplicity, we may idealize the terminal leads as quasi 1-D wires. As waveguides, they can be described in terms of open channels at the Fermi energy or propagating modes. Thus, we chose a basis for the system's Hamiltonian in which each independent propagation mode l of a lead is connected to a single system's state. This might require a unitary transformation to choose a system's basis that matches the propagating modes of leads (see Fig. 1). There is no restriction to the converse: i.e. each "site" can be coupled to different quantum channels. Since the leads can be represented by homogeneous infinite tight-binding chains, their decimation is just the procedure implemented above with the appropriate V's and E's describing each mode l.

The observation of DP was that any "local" electronic state weakly coupled to a huge number of environmental degrees of freedom should decay from its initial decoupled state according to the FGR. This would require a restitution or re-injection of any escaping particle. Thus the DP model treats these decoherent scattering channels sources as on-site fictitious voltage probes. Much as it occurs with real voltmeters, local current conservation on each scattering channels must be imposed. This ensures that each electron with definite energy that escapes from a state towards a fictitious probe, is balanced by an electron *with the same energy* re-injected into the same state. In the DP model, these decoherent channels are described by local corrections to site energies of the sample, on the same footing as the real channels:

$$\hat{\Sigma}_{\phi i} = -i\Gamma_{\phi i}\hat{c}_i^\dagger \hat{c}_i. \qquad (15)$$

Here, $\Gamma_{\phi i}$ represents an energy uncertainty associated with the interaction process ϕ that mixes the local electron state i with environmental degrees of freedom. This introduces a decay of the state i that can be described by the FGR. Notice that the state i does not necessarily represent a local basis, but it could be a channel mode or a momentum basis state as well. The energy uncertainties due to decoherent processes can be estimated for each specific process, [29] and may not necessarily be the same for every state i. Accordingly, each "site" i may be subject to different decay processes α: those associated with real leads, $\alpha = l$, and those related to decoherent processes (or fictitious probes), $\alpha = \phi$. The resulting effective Hamiltonian, $\hat{H}_{\text{eff.}}$, that includes the real and fictitious probes, is non-Hermitian [40]:

$$\hat{H}_{\text{eff.}} = (\hat{H}_S - i\eta\hat{I}) + \sum_\alpha \sum_{i=1}^N \hat{\Sigma}_{\alpha i}. \qquad (16)$$

Here, $\mathrm{Im}\hat{\Sigma}_{\alpha i} \neq 0$ only for those sites i subject to decoherent processes ($\alpha = \phi$) or escapes to the leads ($\alpha = l$). Trivially, if the full imaginary part correction were homogeneous (the same value for each state i), it just shifts
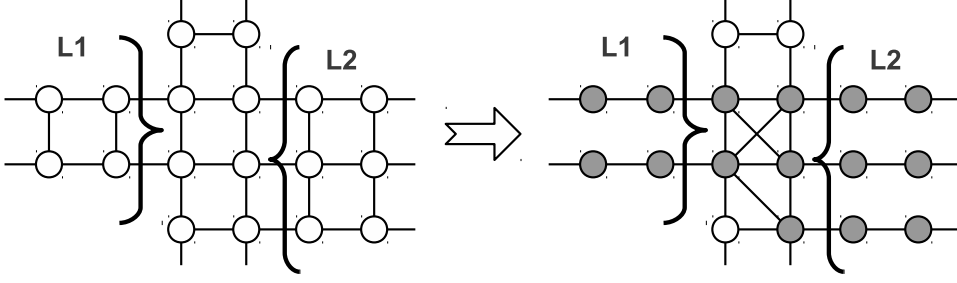
FIG. 1. Diagrammatic representation of an unitary transformation of the system to a basis in which leads are independent. Here, dots represent diagonal elements of the Hamiltonian in a site basis and lines non-diagonal ones.

the eigenenergies into the complex plane. In contrast, inhomogeneous corrections might produce spectral bifucations that result in a quantum dynamical phase transition. [41]

In transport problems, most of the information on system dynamics is distilled into the retarded and advanced Green functions. More practical expressions are obtained using its Fourier transform into the energy variable ε, from the effective Hamiltonian given by Eq. 16. In matrix representation:

$$\mathbb{G}^R(\varepsilon) = [\varepsilon\mathbb{I} - \mathbb{H}_{\text{eff.}}]^{-1} = \mathbb{G}^{A\dagger}(\varepsilon) \qquad (17)$$

These Green's functions contain all the information of the quantum system coupled to the leads and environment and constitute the kernel to move into the non-equilibrium problem. Also, diagonal elements provide the "local" density of states

$$N_i(\varepsilon) = -\frac{1}{\pi}\text{Im}G_{i,i}^R(\varepsilon) = -\frac{1}{2\pi\text{i}}\left[G_{i,i}^R(\varepsilon) - G_{i,i}^A(\varepsilon)\right] \quad (18)$$

In particular, the transmission amplitudes of electronic excitations between the channels identified with process α at site i and process β at site j can be evaluated from the generalized form of Fisher-Lee formula [34]:

$$t_{\alpha i,\beta j}(\varepsilon) = \text{i}2\sqrt{\Gamma_{\beta j}(\varepsilon)}\,G_{j,i}^R(\varepsilon)\,\sqrt{\Gamma_{\alpha i}(\varepsilon)} \qquad (19)$$

and the transmission probabilities are given by:

$$T_{\alpha i,\beta j}(\varepsilon) = |t_{\alpha i,\beta j}(\varepsilon)|^2 \qquad (\alpha i \neq \beta j)$$
$$= 4\Gamma_{\beta j}(\varepsilon)G_{j,i}^R(\varepsilon)\Gamma_{\alpha i}(\varepsilon)G_{i,j}^A(\varepsilon) \qquad (20)$$

where $\Gamma_{\alpha i} = \text{i}(\Sigma_{\alpha,i}^R - \Sigma_{\alpha,i}^A)/2$ is proportional the escape rate at site i due to a process α.

III. TWO-TERMINAL D'AMATO-PASTAWSKI MODEL.

Retarded and advanced Green's functions and the transmission probabilities associated with them contain

the basic quantum dynamics. In order to describe the non-equilibrium properties of a system, one has to evaluate the density matrix or simply the diagonal terms of non-equilibrium density functions,

$$G_{j,j}^<(\varepsilon) = \text{i}2\pi N_j(\varepsilon)\text{f}_j(\varepsilon). \qquad (21)$$

These, in turn, are determined by the boundary conditions imposed by the external reservoirs βj that act as a source or drain of particles. Their occupation is described by a non-equilibrium distribution function approximated by a shifted Fermi distribution $\text{f}_{\beta j}(\varepsilon) = 1/(\exp[(\varepsilon - \varepsilon_F - \delta\mu_{\beta j})/k_BT])$. In the Quantum Fields formalism, the $G_{\phi j,\phi j}^<(\varepsilon)$ Green's functions result from the quantum evolution in presence of the boundary conditions. In the time independent case, energy is conserved, and the non-equilibrium density function takes the form,

$$G_{j,k}^<(\varepsilon) = 2\text{i}\sum_{\alpha i}G_{j,i}^R(\varepsilon)\Gamma_{\alpha i}(\varepsilon)\text{f}_{\alpha i}(\varepsilon)G_{i,k}^A(\varepsilon), \qquad (22)$$

i.e. densities and correlations inside the system result from the occupations $\text{f}_{\beta i}(\varepsilon)$ imposed by the experimentalist at the current terminals and the environment at the "fictitious" probes. The equilibrium density function $G_{j,j}^{(0)<}(\varepsilon)$ results when $\delta\mu_{\beta j} \equiv 0$ for all βj. The actual observables are evaluated from this non-equilibrium density function. The change respect to the equilibrium in the local density can be expressed in terms of the above boundary conditions as [18]:

$$\delta\rho_j = -\frac{\text{i}}{2\pi}\int\left[G_{j,j}^< - G_{j,j}^{(0)<}\right]\text{d}\varepsilon \qquad (23)$$
$$\simeq N_j(\varepsilon_F)\delta\mu_j,$$

while the currents between sites i and j are given by

$$I_{i,j} = \int\left[V_{i,j}G_{j,i}^< - V_{j,i}G_{i,j}^<\right]\text{d}\varepsilon. \qquad (24)$$

These integral expressions of the observables, expressed in the linear response approximation of small biases

$eV_L = \mu_{Li} - \varepsilon_F \ll \varepsilon_F$, become the Generalized Landauer-Büttiker equations that describe the balance of electronic current. These are no other than the Kirchhoff laws expressed in terms of the generalized Landauer's conductances, given by the Fisher-Lee formulas of Eq. 20. Because of the linear approximation these transmittances are evaluated at the Fermi energy, and now become:

$$I_{\alpha i} = \frac{e}{h} \sum_{\substack{\beta = L, \phi \\ \text{processes}}} \sum_{\substack{j=1(\alpha i \neq \beta j) \\ \text{sites}}}^{N} (T_{\alpha i, \beta j} \delta \mu_{\beta j} - T_{\beta j, \alpha i} \delta \mu_{\alpha i}) \tag{25}$$

where the quantities $\delta \mu_{\alpha i} = \mu_{\alpha i} - \varepsilon_F$, are the chemical potentials of the electron reservoirs, at state i for a process α.

The requirement in the DP model that no net current flows through the decoherent channels imposes

$$0 \equiv I_{\phi i}. \tag{26}$$

These equations imply the self-consistent determination of the internal non-equilibrium chemical potentials $\delta \mu_{\phi i}$. Thus, we are faced to a linear problem. Once again, its solution can be laid as a decimation procedure, as we did to obtain the effective Hamiltonian.

Consider the case where two real leads are connected to the sites 1 and N of the system (thus identified as channels $\ell 1$ and ℓN), and a *single* decoherent process ϕk is connected to the state k. Thus, charge conservation implies:

$$0 = T_{\phi k, \ell 1} \delta \mu_{\ell 1} + T_{\phi k, \ell N} \delta \mu_{\ell N} - (T_{\ell 1, \phi k} + T_{\ell N, \phi k}) \delta \mu_{\phi k}, \tag{27}$$

which can be rewritten as:

$$\delta \mu_{\phi k} = \frac{T_{\phi k, \ell N}}{(T_{\ell 1, \phi k} + T_{\ell N, \phi k})} \delta \mu_{LN} + \frac{T_{\phi k, \ell 1}}{(T_{\ell 1, \phi k} + T_{\ell N, \phi k})} \delta \mu_{\ell 1} \tag{28}$$

Using this relation for the current on real channels we obtain:

$$I_{\ell N} = -I_{\ell 1} = \frac{e}{h} \tilde{T}_{\ell N, \ell 1} (\delta \mu_{\ell N} - \delta \mu_{\ell 1}), \tag{29}$$

where $\tilde{T}_{\ell N, \ell 1}$ represent the "effective" transmission between leads $\ell 1$ and ℓN after the decimation of the incoherent channel associated with ϕk, given by:

$$\tilde{T}_{\ell N, \ell 1} = T_{\ell N, \ell 1} + T_{\ell N, \phi k} \frac{1}{(T_{\ell 1, \phi k} + T_{\ell N, \phi k})} T_{\phi k, \ell 1}. \tag{30}$$

Note that the zero current constrain at the decoherent channels allows us to pile up (i.e. decimate) those processes into an incoherent contribution to the total transmission. This is the reason why Eq. 26 is the key factor in the computation of the total transmission. At this point one recognizes the analogy of the second term on the right-hand side of Eq. 30 with the effective interaction shown in Eq. 4. This analogy will be used in the following section to develop a simple matrix solution

for the total decoherent transmission in a multi-terminal setup. In the case of two current probes, identifying the index label $L = \ell 1$ and $R = \ell N$ for the leads, and $\phi k = k$ for the decoherence probes, one has that the total transmission probability is given by:[16]

$$\tilde{T}_{L,R} = T_{L,R} + \sum_{i,j} T_{R,i} \left[\mathbb{W}^{-1} \right]_{i,j} T_{j,L}. \tag{31}$$

The elements of the matrix $\mathbb{W}$ are:

$$W_{ij} = -T_{ij} + \left(\sum_{j=L,i,R} T_{ij} \right) \delta_{ij}. \tag{32}$$

Eqs. 29 and 31 provide the decoherent current and the effective transmission of DP model for two-terminal setups. However, they need to be reformulated to deal with a multi-terminal setup as when there are more than two externally controlled chemical potentials or when one requires to discriminate among different processes that contribute to the current.

IV. MULTI-TERMINAL D'AMATO-PASTAWSKI MODEL

The two-probe Landauer conductance requires the computation of a single element of the Green's function matrix: that connecting sites where the leads are attached. In a 1-D case, this is G_{1N} (where N is the number of sites of the system) and can be calculated through a decimation procedure.[37] While this can be readily generalized to deal with finite systems of any dimension, not all formulations result numerically stable in presence of strong disorder or band gaps.[42] We will present a particular algorithm that is stable in such conditions. The method is applicable to block tridiagonal Hamiltonians. These are very common in many physicaly relevant situations, specifically when interactions are truncated, or when the Hamiltonian matrix presents some form of banded structure.

The DP model requires the computation of the transmittances among all possible pairs of fictitious and physical probes, roughly $M(M-1)/2$, where M ($\leq N$) is the number of phase-breaking scattering channels. Also the computation of the effective transmission requires the inversion of $\mathbb{W}$, a $M \times M$ matrix, as expressed in Eq. 31. It is our purpose to extend the scheme of the DP model to account for decoherence in quantum transport problems that involves many terminals. We seek for a decoherent transmission analogous to Eq. 31 for each pair of physical leads. Thus, the computational approach to the DP model would require an efficient matrix inversion algorithm.

In the next subsection, we present a computational procedure that, being based on decimation schemes, preserves the physical meaning of matrix inversions. This may allow one to take advantage of system's symmetries

as they can usually be expressed as relations between $\mathbb{G}$'s elements.

A. Green's Function and recursive algorithms.

In order to obtain the Green's functions of Eq. 17, a matrix inversion is needed. The *matrix continued fractions* [43, 44] scheme offers a decimative approach well suited to perform this task. This procedure can be constructed recalling the well known 2×2 block matrix inversion,

$$\begin{bmatrix} \mathbb{A} & \mathbb{B} \\ \mathbb{C} & \mathbb{D} \end{bmatrix}^{-1} = \begin{bmatrix} (\mathbb{A} - \mathbb{B}\mathbb{D}^{-1}\mathbb{C})^{-1} & -\mathbb{A}^{-1}\mathbb{B}(\mathbb{D} - \mathbb{C}\mathbb{A}^{-1}\mathbb{B})^{-1} \\ -\mathbb{D}^{-1}\mathbb{C}(\mathbb{A} - \mathbb{B}\mathbb{D}^{-1}\mathbb{C})^{-1} & (\mathbb{D} - \mathbb{C}\mathbb{A}^{-1}\mathbb{B})^{-1} \end{bmatrix}, \tag{33}$$

where $\mathbb{A}$, $\mathbb{B}$, $\mathbb{C}$ and $\mathbb{D}$ are arbitrary size subdivisions of the original matrix.

Let's assume that we have an effective Hamiltonian, $\hat{H}_{\text{eff.}}$ which has block tridiagonal structure. We start "partitioning" the basis states in two portions: a cluster labeled as 1 that contains the first block, and the cluster of remaining states of the system which we label as B. Thus, the Green's function matrix in Eq. 17 is subdivided into four blocks, $(\varepsilon\mathbb{I} - \mathbb{E}_1), (\varepsilon\mathbb{I} - \mathbb{E}_B), -\mathbb{V}_{1B}$, and $-\mathbb{V}_{B1}$ of dimensions $N_1 \times N_1$, $N_B \times N_B$, $N_1 \times N_B$ and $N_B \times N_1$ respectively. Thus,

$$\mathbb{G}(\varepsilon) = \begin{bmatrix} \mathbb{G}_{11} & \mathbb{G}_{1B} \\ \mathbb{G}_{B1} & \mathbb{G}_{BB} \end{bmatrix} = \begin{bmatrix} \varepsilon\mathbb{I} - \mathbb{E}_1 & -\mathbb{V}_{1B} \\ -\mathbb{V}_{B1} & \varepsilon\mathbb{I} - \mathbb{E}_B \end{bmatrix}^{-1}. \tag{34}$$

Here, it is important to recall that the effective Hamiltonian $\hat{H}_{eff.}$ already includes all corrections due to fictitious and real probes, by virtue of Eq. 16. In this way, the block with energies and interactions, denoted here by $\mathbb{E}_i$, contain the self-energies that account for the openness of the system, and may be complex numbers. Combining Eq. 33 and Eq. 34 is easy to show that,

$$\begin{aligned} \mathbb{G}_{11} &= \left(\varepsilon\mathbb{I} - \mathbb{E}_1 - \boldsymbol{\Sigma}_1^{(B)}\right)^{-1} = \left(\varepsilon\mathbb{I} - \tilde{\mathbb{E}}_1\right)^{-1}, \\ \mathbb{G}_{BB} &= \left(\varepsilon\mathbb{I} - \mathbb{E}_B - \boldsymbol{\Sigma}_B^{(1)}\right)^{-1} = \left(\varepsilon\mathbb{I} - \tilde{\mathbb{E}}_B\right)^{-1}, \\ \mathbb{G}_{1B} &= \mathbb{G}_{11}\mathbb{V}_{1B}(\varepsilon\mathbb{I} - \mathbb{E}_B)^{-1} = \mathbb{G}_{11}\left[\boldsymbol{\Sigma}_1^{(B)}\mathbb{V}_{B1}^{-1}\right], \text{ and} \\ \mathbb{G}_{B1} &= \mathbb{G}_{BB}\mathbb{V}_{B1}(\varepsilon\mathbb{I} - \mathbb{E}_1)^{-1} = \mathbb{G}_{BB}\left[\boldsymbol{\Sigma}_B^{(1)}\mathbb{V}_{1B}^{-1}\right]. \end{aligned} \tag{35}$$

Here, the similarity with Eq. 4 allows us to define the block self energies, $\boldsymbol{\Sigma}$'s, which in this simple 2×2 block scheme, are given by:

$$\begin{bmatrix} \boldsymbol{\Sigma}_1^{(B)}\mathbb{V}_{B1}^{-1} \end{bmatrix} = \left[\mathbb{V}_{1B}(\varepsilon\mathbb{I} - \mathbb{E}_B)^{-1}\right], \\ \begin{bmatrix} \boldsymbol{\Sigma}_B^{(1)}\mathbb{V}_{1B}^{-1} \end{bmatrix} = \left[\mathbb{V}_{B1}(\varepsilon\mathbb{I} - \mathbb{E}_1)^{-1}\right]. \tag{36}$$

Notice, that in the expressions of Eqs. 35 and 36, the inverse of the hopping matrix must cancel with the hopping that enters in the self-energies definition. Since the hoppings may be non-square matrices, this definition is crucial to avoid its inversion. Considering the bracket

factors $\left[\boldsymbol{\Sigma}\mathbb{V}^{-1}\right]$ as a single object ensures stability of the recurrence procedure. The decimation of the degrees of freedom associated with the portion B of the effective Hamiltonian is implied in Eq. 35, where:

$$\tilde{\mathbb{E}}_1 = \mathbb{E}_1 + \boldsymbol{\Sigma}_1^{(B)} = \mathbb{E}_1 + \left[\mathbb{V}_{1B}(\varepsilon\mathbb{I} - \mathbb{E}_B)^{-1}\right]\mathbb{V}_{B1}. \tag{37}$$

Likewise, the decimation of block 1 into B gives the effective block:

$$\tilde{\mathbb{E}}_B = \mathbb{E}_B + \boldsymbol{\Sigma}_B^{(1)} = \mathbb{E}_B + \left[\mathbb{V}_{B1}(\varepsilon\mathbb{I} - \mathbb{E}_1)^{-1}\right]\mathbb{V}_{1B}. \tag{38}$$

Note that with the adopted notation for the self energies, $\Sigma_i^{(j)}$ is the correction to block site i when all block sites between i and j (with j included) are decimated. Therefore the supra-index in parentheses indicate the subspace that has been decimated.

Since we are dealing with tridiagonal block matrices, we may resort to a further partition for the matrix inversion involved in Eq. 37. i.e. the block B describes states that can be subdivided into two clusters where the first one, labeled 2, corresponds to the first tridiagonal block from $(\varepsilon\mathbb{I} - \mathbb{E}_B)$. The other block B' now satisfies $\mathbb{V}_{1B'} \equiv \mathbb{O}$. Then, we have

$$\mathbb{G}(\varepsilon) = \begin{bmatrix} \varepsilon\mathbb{I} - \mathbb{E}_1 & -\mathbb{V}_{12} & \mathbb{O} \\ -\mathbb{V}_{21} & \varepsilon\mathbb{I} - \mathbb{E}_2 & -\mathbb{V}_{2B'} \\ \mathbb{O} & -\mathbb{V}_{B'2} & \varepsilon\mathbb{I} - \mathbb{E}_{B'} \end{bmatrix}^{-1}. \tag{39}$$

Again, we can also decimate the degrees of freedom associated with block 2, taking

$$\begin{aligned} \tilde{\mathbb{E}}_1 &= \mathbb{E}_1 + \boldsymbol{\Sigma}_1^{(2)}, \quad \tilde{\mathbb{E}}_{B'} = \mathbb{E}_{B'} + \boldsymbol{\Sigma}_{B'}^{(2)} \\ \tilde{\mathbb{V}}_{1B'} &= \mathbb{V}_{12}(\varepsilon\mathbb{I} - \mathbb{E}_2)^{-1}\mathbb{V}_{2B'} \end{aligned} \tag{40}$$

which leads to an effective equation analogous to Eq. 34, in terms of the new effective block sites:

$$\begin{bmatrix} \mathbb{G}_{11} & \mathbb{G}_{1B'} \\ \mathbb{G}_{B'1} & \mathbb{G}_{B'B'} \end{bmatrix} = \begin{bmatrix} \varepsilon\mathbb{I} - \tilde{\mathbb{E}}_1 & -\tilde{\mathbb{V}}_{1B'} \\ -\tilde{\mathbb{V}}_{B'1} & \varepsilon\mathbb{I} - \tilde{\mathbb{E}}_{B'} \end{bmatrix}^{-1} \tag{41}$$

Therefore, an expression analogous to Eq. 35 is obtained:

$$\mathbb{G}_{11} = \left(\varepsilon\mathbb{I} - \mathbb{E}_1 - \mathbf{\Sigma}_1^{(B')}\right)^{-1}$$
$$\mathbb{G}_{B'B'} = \left(\varepsilon\mathbb{I} - \mathbb{E}_{B'} - \mathbf{\Sigma}_{B'}^{(1)}\right)^{-1}$$
$$\mathbb{G}_{1B'} = \mathbb{G}_{11}\tilde{\mathbb{V}}_{1B'}(\varepsilon\mathbb{I} - \tilde{\mathbb{E}}_{B'})^{-1} \qquad (42)$$
$$\mathbb{G}_{B'1} = \mathbb{G}_{B'B'}\tilde{\mathbb{V}}_{B'1}(\varepsilon\mathbb{I} - \tilde{\mathbb{E}}_1)^{-1}$$

where the diagonal blocks of the Green's function matrix involve

$$\mathbf{\Sigma}_1^{(B')} = \left[\mathbb{V}_{12}(\varepsilon\mathbb{I} - \mathbb{E}_2 - \mathbf{\Sigma}_2^{(B')})^{-1}\right]\mathbb{V}_{12}$$
$$\mathbf{\Sigma}_{B'}^{(1)} = \left[\mathbb{V}_{B'2}(\varepsilon\mathbb{I} - \mathbb{E}_2 - \mathbf{\Sigma}_2^{(1)})^{-1}\right]\mathbb{V}_{2B'} \qquad (43)$$

Note that in the self-energies of Eq. 43, the decimated space (denoted by the supra-index) always includes one of the border blocks (in this case, 1 or B). However, as shown hereafter, the non-diagonal terms can also be written in terms of the block self-energies $\mathbf{\Sigma}^{(1)}$'s and $\mathbf{\Sigma}^{(B')}$'s:

$$\mathbb{G}_{1B'} = \mathbb{G}_{11}[\mathbf{\Sigma}_1^{(B')}\mathbb{V}_{12}^{-1}][\mathbf{\Sigma}_2^{(B')}\mathbb{V}_{B'2}^{-1}],$$
$$\mathbb{G}_{B'1} = \mathbb{G}_{B'B'}[\mathbf{\Sigma}_{B'}^{(1)}\mathbb{V}_{1B'}^{-1}][\mathbf{\Sigma}_2^{(1)}\mathbb{V}_{12}^{-1}]. \qquad (44)$$

Both expressions are crucial to visualize the seed of our recursive procedure.

The generalization by further partition into an arbitrary number of clusters is straightforward. The Green's functions are expressed as a product of non-singular self-energy blocks that are calculated recursively. Independently of how the effective Hamiltonian is subdivided, if there are N blocks of arbitrary size and the entire system is decimated into the i-th and j-th block, we have simply as matrix continued fractions: [44]

$$\mathbf{\Sigma}_i^{(j)} = \left[\mathbb{V}_{i,i+1}\left(\varepsilon\mathbb{I} - \mathbb{E}_{i+1} - \mathbf{\Sigma}_{i+1}^{(j)}\right)^{-1}\right]\mathbb{V}_{i+1,i}$$
$$\mathbf{\Sigma}_j^{(i)} = \left[\mathbb{V}_{j,j-1}\left(\varepsilon\mathbb{I} - \mathbb{E}_{j-1} - \mathbf{\Sigma}_{j-1}^{(i)}\right)^{-1}\right]\mathbb{V}_{j-1,j} \qquad (45)$$
$$\text{for} \quad j > i,$$

provided that the final structure preserves a block three-diagonal. We recall that matrix inversions are further stabilized by the presence of the imaginary site energies imposed by the real and fictitious probes (Eq. 16). In this way, the decimation of the entire system into the arbitrary "block" sites i and j, leads to the effective quantities

$$\tilde{\mathbb{E}}_i = \mathbb{E}_i + \mathbf{\Sigma}_i^{(1)} + \mathbf{\Sigma}_i^{(j)}$$
$$\tilde{\mathbb{E}}_j = \mathbb{E}_j + \mathbf{\Sigma}_j^{(i)} + \mathbf{\Sigma}_j^{(N)} \qquad (46)$$
$$\tilde{\mathbb{V}}_{i,j} = \tilde{\mathbb{V}}_{i,j-1}(\varepsilon\mathbb{I} - \mathbb{E}_j - \mathbf{\Sigma}_j^{(1)})^{-1}\mathbb{V}_{j-1,j}$$

which determine exactly each (i,j) element of the total Green's function,

$$\begin{bmatrix} \mathbb{G}_{ii} & \mathbb{G}_{ij} \\ \mathbb{G}_{ij} & \mathbb{G}_{jj} \end{bmatrix} = \begin{bmatrix} \varepsilon\mathbb{I} - \tilde{\mathbb{E}}_i & -\tilde{\mathbb{V}}_{ij} \\ -\tilde{\mathbb{V}}_{ji} & \varepsilon\mathbb{I} - \tilde{\mathbb{E}}_j \end{bmatrix}^{-1}. \qquad (47)$$

The last expression is similar to Eq. 34, and therefore we have,

$$\mathbb{G}_{ii} = \left[(\varepsilon\mathbb{I} - \mathbb{E}_i) - \mathbf{\Sigma}_i^{(1)} - \mathbf{\Sigma}_i^{(N)}\right]^{-1},$$
$$\mathbb{G}_{jj} = \left[(\varepsilon\mathbb{I} - \mathbb{E}_j) - \mathbf{\Sigma}_j^{(1)} - \mathbf{\Sigma}_j^{(N)}\right]^{-1},$$
$$\mathbb{G}_{ij} = \mathbb{G}_{ii}\left[\tilde{\mathbb{V}}_{ij}(\varepsilon\mathbb{I} - \tilde{\mathbb{E}}_j)^{-1}\right], \qquad (48)$$
$$\mathbb{G}_{ji} = \mathbb{G}_{jj}\left[\tilde{\mathbb{V}}_{ji}(\varepsilon\mathbb{I} - \tilde{\mathbb{E}}_i)^{-1}\right].$$

This procedure is shown diagrammatically on Fig. 2. Note that the diagonal elements are easily calculated evaluating $\mathcal{O}(N)$ energy corrections of the form $\Sigma_i^{(1)}$ and $\Sigma_i^{(N)}$, where all the sites have been decimated into site i. Also, in order to compute all the non diagonal elements of the Green's function matrix in Eq. 42 and 48 we would need to evaluate $\sim N^2$ energy corrections $\mathbf{\Sigma}_i^{(j)}$'s. However, following the insight given in Eq. 44, for tridiagonal block Hamiltonians, the non-diagonal block matrix elements of the Green function can be obtained in terms of the diagonal ones, avoiding the need of the evaluation of $\mathcal{O}(N^2)$ terms $\Sigma_i^{(j)}$'s. In this case, if the Hamiltonian matrix is subdivided in N arbitrary blocks, we have

$$\mathbb{G}_{ij} = \mathbb{G}_{ii}\prod_{\substack{k=i \\ \text{where } i<j}}^{j-1}\left[\mathbf{\Sigma}_k^{(N)}\mathbb{V}_{k+1,k}^{-1}\right], \qquad (49)$$

$$\mathbb{G}_{ji} = \mathbb{G}_{jj}\prod_{\substack{k=j \\ \text{where } i<j}}^{i+1}\left[\mathbf{\Sigma}_k^{(1)}\mathbb{V}_{k-1,k}^{-1}\right]. \qquad (50)$$

Note that now it is not necessary to evaluate any extra $\mathbf{\Sigma}$ in order to calculate $\mathbb{G}_{ij}$ for $i \neq j$, because those self-energies have been already calculated for the diagonal Green's Functions matrix blocks, $\mathbb{G}_{ii}$. This implies that only $\mathcal{O}(N)$ self-energies are required for the calculation of the whole Green's function. These equations can help to take advantage of possible symmetries of the $\mathbb{V}$ and $\mathbf{\Sigma}$ matrices to speed up even more the calculation of Green's Functions.

Although Eqs. 49-50 have been formally written in terms of hopping matrix inverses, $\mathbb{V}^{-1}$, these expressions are accurate even when the hopping matrices are singular. This is because the hopping matrix inverse cancels out with the hopping in the Σ definition, as it can be seen, for example, in Eq. 36. In most cases, $\mathbb{G}_{ij}^R = \mathbb{G}_{ji}^R$, and therefore Eqs. 49 and 50 are equivalent. However, both equations are needed in some cases of quantum pumping [45] or in the presence of magnetic fields. The origin of the extraordinary stability of Eqs. 49-50 can be easily grasped analytically by considering a linear chain with three sites and expressing the self-energies in terms of continued fractions before applying Eq. 44. Explicitly,
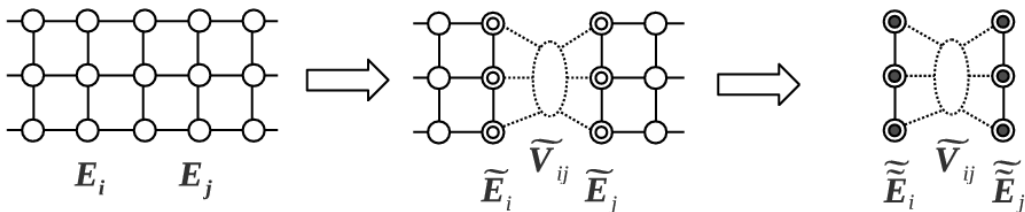
FIG. 2. Decimation scheme for the calculation of the elements of the Green's function matrix.

$$G_{1,3}(\varepsilon) = \cfrac{1}{\varepsilon - E_1 - V_{12}\cfrac{1}{\varepsilon - E_2 - V_{23}\cfrac{1}{\varepsilon - E_3}V_{32}}V_{21}}V_{12}\cfrac{1}{\varepsilon - E_2 - V_{23}\cfrac{1}{\varepsilon - E_3}V_{32}}V_{23}\cfrac{1}{\varepsilon - E_3}. \tag{51}$$

Here, we clearly see that the divergences in the last factor are exactly canceled by the zeros of the second one, while the singularities in this one, are canceled by the zeros in the first factor. This equation holds when the elements E's and V's are replaced by matrices, with $\mathbb{V}_{n,n+1}$'s mixing subspaces $\mathbb{E}_n$ and $\mathbb{E}_{n+1}$ of different dimensions. In general, the divergences in $\left[\boldsymbol{\Sigma}_k^{(N)}\mathbb{V}_{k-1,k}^{-1}\right]$ are compensated by the zeros of the previous term, i.e. $\left[\boldsymbol{\Sigma}_{k-1}^{(N)}\mathbb{V}_{k,k-1}^{-1}\right]$. Furthermore, the regularization of poles and divergencies imposed by decoherent processes (see below) ensure the numerical precision of this cancellation.

B. Physical Observables in the Multi-Terminal D'Amato-Pastawski model

The application of the DP model for multi-terminal devices requires a generalization of Eq. 31. To obtain the total transmission on each terminal, we can take advantage of the decimation procedures discussed above. Eq. 25 is easily rearranged in terms of the transmissivity $(1 - R_{\alpha i})$ from each channel αi. [34] For process α at site i, one defines

$$|t_{\alpha i,\alpha i}|^2 + (1 - R_{\alpha i}) = |t_{\alpha i,\alpha i}|^2 + \sum_{\substack{\beta,j \\ (\beta j \neq \alpha i)}} T_{\beta j,\alpha i} \tag{52}$$

$$= (1/g_{\alpha,i}) = 4\pi N_i \Gamma_{\alpha i}, \tag{53}$$

where N_i is the density of states at the site i. The Fisher-Lee formula is extended by defining a "self-transmission" $|t_{\alpha i,\alpha i}|^2$ that is not a transmittance in the standard sense, and certainly it is not the diagonal term $T_{\alpha i,\alpha i} \equiv R_{\alpha i} - 1$. However, it is required to obtain the sum of Eq. 53 as the product of the local density of states and the decay rate. It describes all the electrons that, at a certain instant, are leaving the αi^{th} reservoir to eventually return after wandering around. The inclusion of this term is important

because it contributes to define $(1/g_{\alpha,i})$, which plays a central role in a Keldysh perturbative expansion [17, 34] and in a time dependent formulation of transport. [18]

Therefore, in a steady state calculation is enough to express eq. 25 as:

$$I_{\alpha i} = \frac{|e|}{h}\left[(R_{\alpha i} - 1)\delta\mu_{\alpha i} + \sum_{\beta=L,\phi}\sum_{\substack{j=1 \\ \alpha i \neq \beta j}}^N T_{\alpha i,\beta j}\delta\mu_{\beta,j}\right]. \tag{54}$$

It can be arranged in a compact matrix notation, separating the processes associated with the leads from the decoherent ones. The actual currents at the leads are arranged in the vector $\overrightarrow{I}_\lambda$ while the vanishing currents at the decoherent channels, in $\overrightarrow{I}_\phi \equiv \overrightarrow{0}$. Thus,

$$\begin{pmatrix} \overrightarrow{I}_\lambda \\ \overrightarrow{0} \end{pmatrix} = \frac{|e|}{h}\mathbb{T}\begin{pmatrix} \delta\overrightarrow{\mu_\lambda} \\ \delta\overrightarrow{\mu_\phi} \end{pmatrix}. \tag{55}$$

Here, the non-diagonal elements of $\mathbb{T}$ are transmission probabilities and thus, they are definite positive. In contrast, the diagonal elements are negative. Thus, a sum over any column or row cancels out. This matrix can also be subdivided in the same block structure:

$$\mathbb{T} = \begin{bmatrix} \mathbb{T}_{\lambda\lambda} & \mathbb{T}_{\lambda\phi} \\ \mathbb{T}_{\phi\lambda} & \mathbb{T}_{\phi\phi} \end{bmatrix}. \tag{56}$$

This notation stress that $\mathbb{T}_{\lambda\lambda}$ only involves terms that connect real leads, $\mathbb{T}_{\phi\phi}$ only involves transmissions between decoherent channels and, finally, the blocks $\mathbb{T}_{\lambda\phi}$ and $\mathbb{T}_{\phi\lambda}$ connect leads with decoherent processes. Thus, both λ and ϕ subscripts may be vectors themselves indicating processes (current leads ℓ or dephasing processes ϕ) and states in the system ($n = 1, ...N$). For instance, for a system with a single resonant state identified as 1 coupled to two terminals and a single decoherent process, $\lambda = (L1, R1)$ and $\phi = \phi 1$. The fact that on-site chemical

potentials at decoherent channels ensure that no net current flows through them, allows us to evaluate $\overrightarrow{\delta\mu_\phi}$, from Eq. 55:

$$\overrightarrow{\delta\mu_\phi} = [-\mathbb{T}_{\phi\phi}]^{-1}\,\mathbb{T}_{\phi\lambda}\overrightarrow{\delta\mu_\lambda}. \tag{57}$$

Here, $\overrightarrow{\delta\mu_\phi}$ provides the chemical potential profile at the sites undergoing decoherence. Notice that, if used in a local space representation, these chemical potentials do not distinguish left from right going electrons. Thus they induce momentum relaxing decoherence. [17, 46, 47]

The decimative procedure involves a simple algebraic relation between the real channels of the system and the chemical potentials associated with currents drains or sources. From Eq. 55, it is straightforward to isolate $\overrightarrow{I}_\lambda$, arriving to the expression:

$$\overrightarrow{I}_\lambda = \frac{e}{h}\widetilde{\mathbb{T}}_{\lambda\lambda}\overrightarrow{\delta\mu_\lambda}, \tag{58}$$

and therefore, the adimensional effective conductances are the non-diagonal elements of the matrix

$$\tilde{\mathbb{T}}_{\lambda\lambda} = \mathbb{T}_{\lambda\lambda} + \mathbb{T}_{\lambda\phi}[-\mathbb{T}_{\phi\phi}]^{-1}\mathbb{T}_{\phi\lambda}, \tag{59}$$

where the first term represents the coherent transmissions while the second involves all the possible transmissions undergoing at least one decoherent process. This last term, involves the inversion of a typically big $N \times N$ matrix. Notice that the matrix in square brackets would correspond to $\mathbb{W}$ in the original D'Amato and Pastawski's paper, see Eq. 31. [16] However, the matrix inversion can be performed resorting to a recursive decimation of the N dephasing channels, taken one by one. Starting from the first one, at each stage of decimation, all the remaining probes and dephasing channels become renormalized according to the following recursive scheme for the matrix elements of $\tilde{\mathbb{T}}$:

$$\tilde{T}_{ij}^{[0]} = T_{ij} \tag{60}$$

$$\tilde{T}_{ij}^{[k]} = \tilde{T}_{ij}^{[k-1]} + \tilde{T}_{i,k}^{[k-1]}\frac{-1}{\tilde{T}_{k,k}^{[k-1]}}\tilde{T}_{k,j}^{[k-1]}. \tag{61}$$

Here, k runs over the dephasing channel index $\phi1...\phi N$ and $\tilde{T}_{ij}^{[k]}$ stands for the matrix element i,j (each of them take the values $\{\ell1...\ell M, \phi1,..., \phi N\}$) of matrix $\mathbb{T}$, after the decimation of k incoherent channels. This recursion algorithm could become particularly useful when only the effective transmission among a few external channels is needed.

Once that all of them were decimated, we have an effective transmission matrix $\tilde{\mathbb{T}} \equiv \tilde{\mathbb{T}}^{(N)}$ given by:

$$\widetilde{\mathbb{T}} = \begin{bmatrix} \tilde{R}_{\ell1} - 1 & \tilde{T}_{\ell1,L2} & \cdots & \tilde{T}_{\ell1,\ell M} \\ \vdots & \vdots & \ddots & \vdots \\ \tilde{T}_{\ell M,\ell1} & \tilde{T}_{\ell M,\ell2} & \cdots & \tilde{R}_{\ell M} - 1 \end{bmatrix} \tag{62}$$

which accounts for the overall (coherent plus incoherent) transmission through the system between different current channels. This effective transmission matrix relates real currents on each site of the sample with the voltages associated with each electron reservoir. It should by noticed that sums over rows or columns, both on the original $\mathbb{T}$ and on $\tilde{\mathbb{T}}$, must be zero, in accordance to the Kirchhoff law.

At this point there is a particular situation that should be discussed: a unique voltage difference between two channel sets. This results in a single chemical potential difference. For example, assuming that all the channels associated with a current source in the "left" source L have the same chemical potential, $\delta\mu_L$ and all those in the current sink R, have $\delta\mu_R$. We can rewrite the net current as:

$$\mathtt{I} = \sum_i I_i = \frac{e}{h}\sum_j^{M_R}\sum_i^{M_L}\tilde{T}_{Rj,Li}(\delta\mu_L - \delta\mu_R) \tag{63}$$

$$= \mathrm{Tr}\left[4\mathbf{\Gamma}_R\mathbb{G}_{N1}^R\mathbf{\Gamma}_L\mathbb{G}_{1N}^A\right](\delta\mu_L - \delta\mu_R) \tag{64}$$

$$= \mathtt{GV} \tag{65}$$

where $\mathtt{G}$ is the effective conductance, $\mathtt{V} = (\delta\mu_L - \delta\mu_R)/e$ is the applied voltage. Notice that Γ_L and Γ_R are square matrices with dimensions $M_L \times M_L$ and $M_R \times M_R$ associated with the $M = M_L + M_R$ quantum channels at the leads L and R. Since the final expression is the trace of a matrix product, the result does not depend on the chosen basis.

For the most general case of several chemical potentials, Eqs. 63-65 can not be used and one should rely on Eqs. 58 and 59 that are the general solution to the multi-terminal DP model. These are the main results of this work together with the algorithms for the Green's functions, Eqs. 50 and 49, and for the effective transmittances, Eqs. 60 and 61. All of them will be tested in physically relevant situations in the next two sections.

V. APPLICATION: DECOHERENCE IN A MODEL FOR A SASER

The explicit description of vibrational degrees of freedom in a transport problem requires a multichannel formulation even in a two probe configuration. This is because one must resort to a Fock-space representation of the Hamiltonian describing electrons and phonons. This situations occur in vibrational spectroscopy[48, 49], polaronic models,[50, 51] photon-assisted tunneling [52, 53] as well as in time-dependent classical electromagnetic fields in Floquet representations.[54]

We will analyze a simple model that represents this family of problems: independent electrons tunneling through a resonance where they are strongly coupled to a quantized vibrational mode. In particular, we describe the optical phonon-assisted tunneling in a double barrier device. It manifests as a satellite peak in the I-V curve. This mechanism led to one [55] of the various proposals for a phonon laser (SASER).[56] In such proposal, a substantial part of the electrons contributing to the current emit an optical phonon. This constitute the

basis for a coherent ultrasound source. [57, 58]. The efficiency of the device depends on the contrast between the satellite peak and the valley, which in turn is determined by specific quantum interferences among the participating channels. Thus, we will explore if these interferences survive the decoherence induced by the acoustic phonons.
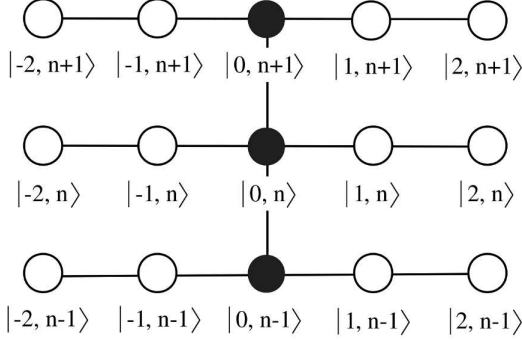

FIG. 3. Fock-space representation of states $|j, n\rangle$. The middle row represents local electronic states j with n phonons. Lower and upper rows describe the same electronic tight-binding chain but with different numbers of phonons. Vertical lines are local electron-phonon couplings restricted to site 0th.

Model. Consider a "local" electronic resonant state labeled as 0. There, the electron is coupled to a single vibrational mode, with frecuency ω_0, whose occupation is associated with the bosonic number operator $\hat{b}^\dagger \hat{b}$. This is represented by the electron-phonon Hamiltonian,

$$\hat{H}_S = E_0 \hat{c}_0^+ \hat{c}_0 + \left(\hbar\omega_0 + \tfrac{1}{2}\right)\hat{b}^+\hat{b} + V_g(\hat{b}^+ + \hat{b})\hat{c}_0^+\hat{c}_0. \quad (66)$$

The eigenstates of this Hamiltonian are the polaron states,[59, 60] whose eigenenergies are

$$E_{0,n} = E_0 + \hbar\omega_0\left(n + \frac{1}{2}\right) - \frac{|V_g|^2}{\hbar\omega_0}. \quad (67)$$

The electrons can jump *in* and *out* the resonant state to the left and right leads. They can also suffer decoherent processes with a rate $2\Gamma_\phi/\hbar$ in a FGR approximation. The effective Hamiltonian results:

$$\hat{H}_{\text{eff}} = \hat{H}_S + \hat{\Sigma}_L + \hat{\Sigma}_R + \hat{\Sigma}_\phi, \quad (68)$$

where $\hat{\Sigma}_L$ and $\hat{\Sigma}_R$ describe the escape to the current leads and $\hat{\Sigma}_\phi$ the escape associated with decoherence. They are,

$$\hat{\Sigma}_L + \hat{\Sigma}_R + \hat{\Sigma}_\phi = \left[\Sigma_L(\varepsilon) + \Sigma_R(\varepsilon) - i\Gamma_\phi\right]\hat{c}_0^+\hat{c}_0. \quad (69)$$

Notice that, these self-energies must account for the high voltage difference required by SASER operation as an offset in the band centers of the left and right leads $E_L - E_R = e\mathsf{V}$. We have omitted a real part of the decoherent process which is not relevant in the present case. As

discussed before [57], the optical phonon absorption and emission can be viewed as a "vertical" processes in a two-dimensional network. Thus, transport in the Fock space is computationally equivalent to a tight-binding model with an expanded dimensionality, as shown in Fig. 3.[50, 57, 59]

When an electron comes from the left side, it arrives at the resonant site where it couples to the n_0 phonons present in the well. It can either keep its original kinetic energy $\varepsilon - \left(n + \frac{1}{2}\right)\hbar\omega_0$ or change it by emitting or absorbing Δn phonons. Thus, the transmission probabilities of each contribution are given by:

$$T_{R(n_0+\Delta n), Ln_0} = 2\Gamma_{R(n_0+\Delta n)}G^R_{n_0+\Delta n, n_0} 2\Gamma_{Ln_0}G^A_{n_0, n_0+\Delta n}. \quad (70)$$

Notice that the subscripts represent channels in the Fock space. As a consequence of the trivial energy shift, associated with the presence of phonons,

$$\Gamma_{\alpha n}(\varepsilon) = \Gamma\left(\varepsilon - E_\alpha - \left(n + \tfrac{1}{2}\right)\hbar\omega_0\right), \quad (71)$$

for $\alpha = L, R$, as defined in Eqs. 9-12. Voltages are accounted by E_α. Each of this processes contributes to the total coherent transmission which is given by,

$$T_{RL}(\varepsilon) = \sum_{\Delta n = -n_0}^{\infty} T_{n_0+\Delta n, n_0}(\varepsilon). \quad (72)$$

In an actual device, the current would be obtained integrating ε with the appropriate Fermi functions. Here, we might recall that Ref. [61] suggested that in the Fock space, "vertical" hoppings could be blocked by the presence of other electrons arriving with different initial energies. However, when the kinetic energy of the incoming electrons satisfies $E_F \leq \hbar\omega_0 \leq e\mathsf{V}$, the applied voltage always enables phonon emission [50, 57, 59] ruling out the eventual problem of overflow [62] ensuring the physical significance of our model.

The decoherence is induced by the finite lifetime for the polaron states through an imaginary correction in the self-energies of Eq. 15. The available "direct" channels are associated with the transmission probabilities of Eq. 70. Because of the wide band approximation for the dephasing channels, the energy uncertainty is independent of ε:

$$\Gamma_{\phi n}(\varepsilon) \equiv \Gamma_\phi. \quad (73)$$

Optical phonon emission or absorption processes give rise to decoherent processes, even when $\Gamma_\phi = 0$. This leaves us with several possible dephasing channels, whose transmittances are

$$T_{\beta(n_0+\Delta n), \alpha n_0} = 2\Gamma_{\beta(n_0+\Delta n)}(\varepsilon)|G^R_{n_0+\Delta n, n_0}(\epsilon)|^2 2\Gamma_{\alpha n_0}(\varepsilon). \quad (74)$$

Here α, β are either R, L or ϕ. From these transmissions, and using Eqs. 59 and 62, we obtain the effective transmissions through the available real channels. Instead of using the SASER operation regime ($n_0 \gg 1$), for pedagogical reasons we will assume that injected electrons find
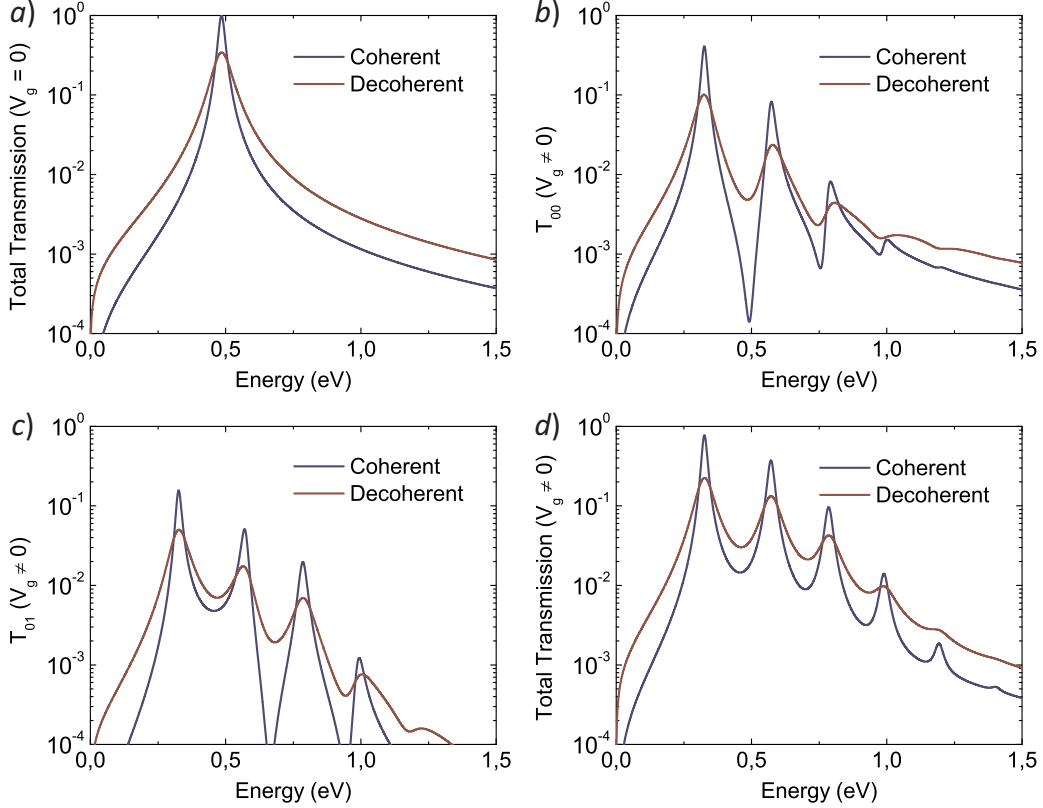
FIG. 4. Multichannel decoherent transmission for the polaron model, with $\hbar\omega_0 = 0.2$ eV, $E_0 = -1.5$ eV. (a) Local electronic state without coupling with the phonons ($V_g = 0$); (b) Transmission probability for an electron leaving the sample without a change in the phonon state ($V_g = 0.1$); (c) Transmission probability for an electron that leaves the sample emitting one phonon ($V_g = 0.1$); (d) Total decoherent transmission probability

$n_0 = 0$ phonons, a situation that describes a vibrational spectroscopy experiments. Then the total transmission is simply,

$$\tilde{T}_{LR}(\varepsilon) = \sum_{n=0}^{N} \tilde{T}_{LR}^{(n)}(\varepsilon), \tag{75}$$

where each $\tilde{T}_{LR}^{(n)}$ includes the decimation of the incoherent channels as in Eq. 30. In what follows we will analyze $\tilde{T}_{LR}(\varepsilon)$ which is also the relevant quantity to study the non-linear response (see Eq. 134 in Ref. [34]).

The total transmission as function of energy is shown in Fig. 4. The Hamiltonian parameters are roughly representative of a double-well resonant tunneling devices where electron-phonon interactions manifest as a satellite peak in the conductance. [55] There $E_0 = -1.5$ eV, $V_R = V_L = -0.1$ eV, $\hbar\omega_0 = 0.2$ eV and $V_g \simeq -0.1$ eV. We discriminate among different vertical processes contributing to the total transmittance. When the coupling between the local electronic state and the phonon mode is neglected, $V_g = 0$, the problem becomes one dimensional with a unique resonance, as shown in Fig. 4-a. The effect of the environment, accounted with the DP model, is a broadening of the original resonance. When the local

electronic state is strongly coupled with the phonon field, $|V_g| \gg 0$, there are extra available paths for the conduction electrons in the Fock space. Different electron pathways in the coherent picture can interfere destructively, e.g. those that traverse the resonance straight away and those that previously emit and absorb a virtual phonon. These give rise to anti-resonances in Figs. 4-b and 4-c. Since they are a coherent phenomena, they may be destroyed when decoherent events are present. This is made evident in Fig. 4-d where the total electron transmission probability in a multi-phonon process is compared with the same configuration with added decoherence, according to the multi-terminal DP model.

The energy uncertainty used is $\Gamma_\phi = 0.026$ $eV \sim k_B T_R$, where k_B is the Boltzmann constant and T_R stands for room temperature of $300K$. Although one might evaluate Γ_ϕ from the electronic energy uncertainties obtained with the help of ab-initio computations, the behavior of $\tilde{T}$ as a function of Γ_ϕ is smooth, provided that these local uncertainties are small compared with typical tunneling rates from the local resonances, $\Gamma_{L(R)} \gg \Gamma_\phi$. Therefore, small variations of the precise value of Γ_ϕ do not change the general behavior of $\tilde{T}$. This is illustrated in Fig. 5 where

a color map shows how Γ_ϕ affects the total transmission probability in the range [0 eV, 0.025 eV]. We confirmed
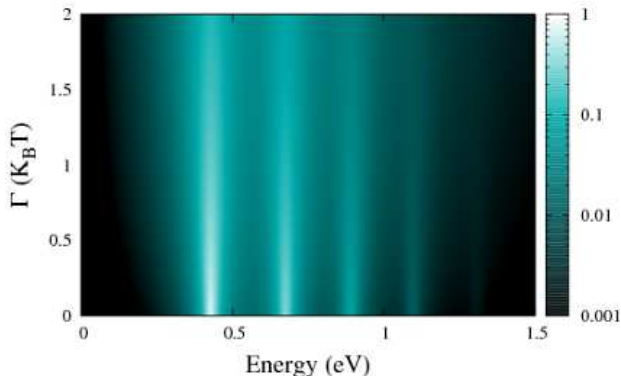

FIG. 5. Multichannel decoherent transmission for the polaron model in a color map. The transmission probability is shown in a color scale, as a function of the incident electron Fermi energy and the strength of the imaginary energy shift Γ_ϕ. The behavior of $\tilde{T}$ is shown to be a smooth function of Γ_ϕ.

the general trend that decoherence broadens and lowers the resonance peaks and raise the tails. But more importantly, valleys are shaped by multi-phonon coherent processes that produce anti-resonances. These resulted very sensitive to decoherence. Thus, these effects should be considered in assessing the efficiency of a SASER.

VI. APPLICATION: QUANTUM TO CLASSICAL TRANSITION IN A MODEL FOR GIANT MAGNETORESISTANCE.

Spintronics often requires to distinguish how each spin projection contribute to the current and to identify the spin dependent voltage profiles, i.e. the chemical potentials $\delta\mu$'s. These are absent from the original solution of the DP model that just provides the total current, $I_{LR} = (e/h)T_{eff}\delta\mu$ (see section III). This limitation was overcome by the previous sections, where a specific current I_j, at spin-channel j, can be readily calculated from eq. 55, as $I_j = e/h \sum_i (\mathbb{T})_{ji} \delta\mu_i$.

Spin-dependent electron transport in ferromagnetic metals presents high rates of scattering events that could make a fully coherent treatment somewhat unrealistic. The standard approach is to use the semiclassical Boltzmann equation [63]. However, in these models quantum mechanic effects are completely neglected from the very beginning. These effects can become important and interesting to study. For instance, ref. [64] shows that spin-dependent transmittances in nanowires with a modulated magnetic field may present Rabi oscillations. In these situations, a Hamiltonian model capable of reach-

ing a semiclassical limit, such as the DP, can be very useful.

In this section, we use the multi-terminal DP model to treat one of the paradigmatic phenomena of the spintronics, the Giant Magnetoresistance (GMR). We will show that one can go from a purely quantum regime, described by a Hamiltonian, to the (semi)classical limit of GMR, just by varying a single parameter: the 'decoherent' scattering rate.

Giant Magnetoresistance may occur in systems composed of two layers of a ferromagnetic metal where their relative magnetization can be switched. In these materials, the rate of scattering depends on the electron spin. Thus, the electrical resistance depends on the relative orientation between the spin and the layer's magnetization. If the two layers have their magnetization aligned, there is a spin orientation with low resistance that dominates transport. On the other hand, when the magnetizations are anti-aligned, both spin channels have high resistance. [33]

Model. Let us consider a one-dimensional system composed of two adjacent 'layers' or portions of a single-domain ferromagnetic metal. We choose the relative magnetization in a anti-aligned configuration (Fig. 6-a). This system is connected to non-magnetic contacts at each side, labeled by L and R. Thus, the current flows perpendicular to the magnetic interface. As usual, each spin is regarded as an independent channel at the contacts. Thus, at the leads, each spin projection is characterized by the chemical potentials $\mu_{L\uparrow}$, $\mu_{L\downarrow}$, $\mu_{R\uparrow}$, and $\mu_{R\downarrow}$. Since we are considering non-ferromagnetic contacts, the chemical potentials at the leads are spin independent.

Inside the system, the electrons undergo scattering processes producing the spin dependent resistance. Since its fair to neglect Anderson localization, we can use the equivalence between delta function impurities and local decoherent scattering processes. As in the Ohmic limit of the DP model [16, 17] they can be characterized by the parameter Γ_ϕ. This is related with the mean free time, τ_σ, through $\Gamma_\sigma = \hbar/(2\tau_\sigma)$. Then, the Ohmic conductance is proportional to the mean free path ℓ_σ which results $\ell_\sigma = v_F\tau_\sigma$. Note that the rate Γ_σ depends on the relative orientation between the spin and the local magnetization. Thus, spin $\uparrow$ has a scattering rate $\Gamma_{\phi 1}$, at the first layer, and $\Gamma_{\phi 2}$, at the second one. The opposite spin has the complementary rates.

As in previous works,[64, 65] the system's Hamiltonian $\hat{H}_S$ is described in a tight-binding approach that includes local spin-reversing interactions:

$$\hat{H}_S = \sum_{i=-N}^{N} \sum_{\sigma=\uparrow,\downarrow} [E_{i,\sigma}\hat{c}_{i,\sigma}^\dagger\hat{c}_{i,\sigma} + V \left[\hat{c}_{i\sigma}^\dagger\hat{c}_{i+1\sigma} + \text{c.c.}\right]$$
$$+ \sum_{i=-N}^{N} V_{\downarrow\uparrow} \left[\hat{c}_{i\downarrow}^\dagger\hat{c}_{i\uparrow} + \text{c.c.}\right]. \tag{76}$$

The label i indicates sites on a lattice with unit cell a,

$E_{i,\sigma}$ is the energy at the site i with spin σ, the operator $\hat{c}_{i,\sigma}^{\dagger}$ ($\hat{c}_{i,\sigma}$) creates (annihilates) a particle at the site i with spin σ. The firsts two terms of $\hat{H}$ accounts for the site energies and the spin-conserving hopping, V, between adjacent sites. V is chosen as the unit of energy. In a graphical representation, each spin orientation is represented by a chain of sites interconnected by V. Thus, two chains of sites are needed to represent the spin-dependent transport along this ferromagnetic system (Fig. 6-a)). The last term of $\hat{H}$, models the scattering processes that may change the spin projection, such as scattering with magnetic impurities. Thus, $V_{\downarrow\uparrow}$ is the local spin-reversing or spin-mixing hopping parameter. This is related to a characteristic length scale identified as the spin diffusion length, L_{sd}, by

$$L_{sd} = \frac{\hbar v_F}{2\,|V_{\downarrow\uparrow}|}, \qquad (77)$$

where v_F is the Fermi velocity and L_{sd} is the length scale at which the spin-flipping processes relax the diffusing spin. Thus, within this length, both spin orientations can be considered as independent. L_{sd} is typically much larger than the mean free path. When the electron gets into the ferromagnetic material, it undergoes an *exchange interaction* that can be regarded as a Zeeman interaction. Thus, the site energy is $E_{i,\uparrow(\downarrow)} = E_0 \pm \Delta E_Z$, where i is a site of the first layer.

As in Eq. 16, the effective Hamiltonian incorporates the leads and the scattering processes through the appropriate self-energies. Now, $\hat{\Sigma}_{L(R)} = \hat{\Sigma}_{L(R)\uparrow} + \hat{\Sigma}_{L(R)\downarrow}$ is the self-energy operator describing the escape to the left (right) lead, given by Eq. 9, where all hoppings are equal to V. Decoherent channels accounting for resistive scattering are associated to each site and included into $\hat{H}$ through the $\hat{\Sigma}_\phi$ operator. Thus, $\hat{\Sigma}_\phi$ is diagonal in a matrix representation. In the wide band limit, their elements are purely imaginary, i.e. $\left(\hat{\Sigma}_\phi\right)_{ii} = -i\Gamma_{\phi i}$.

Classical regime of GMR: two resistors model (TRM). Here, the system length is much shorter than L_{sd}, i.e. $V_{\downarrow\uparrow} \approx 0$ in Eq. 76. Here, when electrons enters into a ferromagnetic layer they undergo an electrical resistance $\delta R = I_{LR}V$ (Ohm's law) that manifest in a linear drop in the chemical-potential $\delta\mu$. Therefore, in the anti-aligned configuration, there are two linear potential drops of $\delta\mu$ with slopes proportional to the spin-dependent resistance of each layer. Then, it is expected a splitting of the chemicals potentials that form a diamond like figure. This is precisely what we obtain using the multi-terminal DP method with mean free paths shorter that the system size. Fig. 6-b to 6-d show this, through the site-dependent chemical potential. In contrast, for the quantum limit of long mean free paths, quantum interferences are evident. However, they are smoothed out by increasing the scattering rate until they reach the expected classical diamond like figure (Fig. 6-b).

Semiclassical regime of GMR: Valet and Fert theory. Considering finite values for the spin diffusion length,
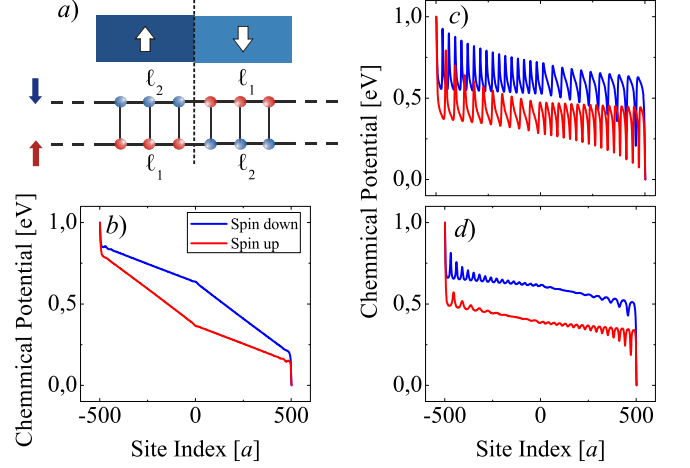

FIG. 6. -a) On top is a scheme showing the layer's magnetization in the two resistor model for GMR. Below is a tight binding representation discriminating the spin projection. The coherence lengths of electrons in the first layer are ℓ_1 and ℓ_2 for up and down spin electrons respectively. Note that coherence lengths are inverted in the next layer. $\ell_1/\ell_2 = 1/2$ in all cases. Fig. b) to d) Site dependent chemical potentials with $\ell_1 = 15\,a$ in Fig. b), $\ell_1 = 1500\,a$ in Fig. c), and $\ell_1 = 150\,a$ in Fig. d). The system length is $1000a$ and $V_{\downarrow\uparrow} = 0$ ($L_{sd} \to \infty$), and the chemical potentials at the leads are $\mu_L = e$V and $\mu_R = 0$. The Fermi wavelengths at the left side are $\lambda_F = 45a$, for up spins, and $\lambda_F = 30a$, for down spins. The opposite holds at the right ferromagnet. The chosen parameters do not represent a specific experimental set up.
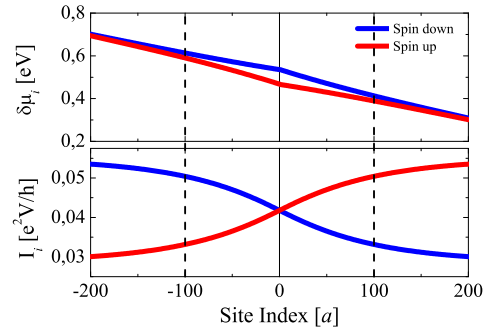

FIG. 7. Upper figure, site-dependent chemical potential $\delta\mu_i$ profile for the semiclassical model of GMR with finite spin diffusion length, $L_{sd} = 100\,a$. Lower figure, shows the local currents I_i for up and down spin electrons. System size is $1000a$, $\ell_1/\ell_2 = 1/2$, and $\ell_1 = 15a$.

L_{sd}, Valet and Fert [63] showed that the difference of the spin-dependent local chemical potentials decays exponentially with the distance to the magnetic interface with a length scale given by L_{sd}. They also showed that the spin-dependent current is inverted in this length scale. In Fig 7 we show that the multi-terminal DP model is also capable to reproduce these behaviors provided that we turn on the spin flip term in Eq. 76. In the up-

per figure we show the spin and site dependent chemical potentials. One can see that in regions far from the interface, distances larger than L_{sd}, the chemical potentials are nearly the same. In regions close to the interface, the chemical potential drop forms a diamond-like figure that show the expected spin-dependent exponential contributions summed up to the trivial mean linear drop. In the lower figure we can observe how the inversion of the currents is produced in the length scale L_{sd}. For longer distances, the currents reach a stationary value.

All these behaviors are in agreement with Ref. [63]. This situation reinforces the descriptive conceptual value of the DP model and the versatility of the numerical algorithms developed in this paper.

VII. CONCLUSION

In this work, we first reviewed the original two-terminal DP model, which accounts for decoherent effects in quantum transport. Then, we presented an extension of this model which is capable to deal with multi-terminal setups. Also, we introduced recursive algorithms that allows us to take advantage of the problem symmetries, in particular in the case of general banded Hamiltonians. The incorporation of a unified notation gives more transparency to its potentialities. Using the specific Hamiltonian models for phonon laser and giant magnetoresistance, we exemplified how to treat multi-channel problems in presence of decoherence.

We made special emphasis on the role of decimation procedures in the context of banded effective Hamiltonians, since they can be used as the basis for efficient computational schemes. In particular, one of the keys is given by Eqs. 49- 50. Note that, in the very common situation of block tridiagonal (i.e. banded) matrix Hamiltonians, these recursive equations provide an efficient decimation procedure that allows one to obtain all the $N \times (N-1)$ non-diagonal blocks of the whole Green's function matrix, $\mathbb{G}$, in terms of the N diagonal blocks. In turn, these last can be calculated as matrix continued fractions. [44] The idea here is to take advantage of particular system's symmetries using these expressions to build an efficient computation approach for the problem under study.

Profiting from a parallelism between the computation of $\mathbb{G}$ and the decoherent transmitance $\tilde{\mathbb{T}}$ already hinted by the DP solution [17], we also derived a compact matrix equation for $\tilde{\mathbb{T}}$ in a generalized multi-terminal scheme. This recursive algorithm relies on decimation procedures.

As a first application, we added decoherent processes to the usual model for phonon-assisted tunneling in the configuration used for a phonon laser or SASER. As is well known, [55] in the I-V curve of a SASER configuration, the contrast between the valley (out of resonance) and the satellite peak (corresponding to phonon emission) is enhanced by the effect of antiresonances. These last result from the interference between different paths in the Fock's space. [57] Besides of the expected smoothing out of the resonances because of the decoherence, we found that it leads to the degradation of the contrast mainly from the suppression of the antiresonances. This could set up new bounds for the efficiency of SASER operation. [58]

We also solved a simple multi-terminal DP model representative of the giant magnetoresistance (GMR) phenomenon. There, each spin orientation is a different conduction channel. Thus, the spin-dependent transport is intrinsically multi-terminal. We essentially showed that the main characteristics of the GMR can be well reproduced with this simple model. While preserving a Hamiltonian description, it is able to reach the expected classical and semiclassical regimes by means of a single parameter, the local decoherent rate $\Gamma_{\phi i}$. What is more important, as in Fig. 6-c and d, it opens the possibility to profit from situations where quantum interference becomes relevant. [64, 66]

With increasing system's size, molecular electronics suffers a paradigm shift on its dominant transport mechanism, from "coherent tunneling" to "incoherent hopping". Within this context, the present work should result specially helpful in providing a computational bridge between these limiting situations, while maintaining a general, transparent, and efficient approach to quantum transport.

VIII. ACKNOWLEDGMENTS

[1] A. Pecchia and A. Di Carlo, Rep. Prog. Phys. **67**, 1497 (2004)

[2] N. A. Zimbovskaya and M. R. Pedersonc, Phys. Rep. **509**, 1 (2011)

[3] G. Cuniberti, G. Fagas, and K. Richter, *Introducing molecular electronics: A brief overview*, Lecture Notes in Physics (Springer Berlin Heidelberg, 2005) ISBN 978-3-540-27994-5

[4] W. Liang, M. Bockrath, D. Bozovic, J. H. Hafner, M. Tinkham, and H. Park, Nature **411**, 665 (2001)

[5] S. P. Giblin, M. Kataoka, J. D. Fletcher, P. See, T. J. B. M. Janssen, J. P. Griffiths, G. A. C. Jones, I. Farrer, and D. A. Ritchie, Nat. Commun. **3**, 930 (2012)

[6] A. Nitzan and M. A. Ratner, Science **300**, 1384 (2003)

[7] R. Bustos-Marún, G. Refael, and F. von Oppen, Phys. Rev. Lett. **111**, 060802 (2013)

[8] P. Rickhaus, R. Maurand, M.-H. Liu, M. Weiss, K. Richter, and C. Schönenberger, Nat. Commun. **4**, 2342 (2013)

[9] C. George, I. Szleifer, and M. Ratner, ACS Nano **7**, 108 (2013)

[10] M. B. Plenio and S. F. Huelga, New J. Phys. **10**, 113019 (2008)

[11] P. Rebentrost, M. Mohseni, I. Kassal, S. Lloyd, and A. Aspuru-Guzik, New J. Phys. **11**, 033003 (2009)

[12] D. J. Thouless and S. Kirkpatrick, J. Phys. C: Solid State Phys. **14**, 235 (1981)

[13] Y. Imry and R. Landauer, Rev. Mod. Phys. **71**, S306 (1999)

[14] M. Büttiker, Phys. Rev. Lett. **57**, 1761 (1986)

[15] M. Büttiker, Phys. Rev. B **33**, 3020 (1986)

[16] J. L. D'Amato and H. M. Pastawski, Phys. Rev. B **41**, 7411 (1990)

[17] H. M. Pastawski, Phys. Rev. B **44**, 6329 (1991)

[18] H. M. Pastawski, Phys. Rev. B **46**, 4053 (1992)

[19] P. Danielewicz, Ann. Phys. **152**, 239 (1984)

[20] L. Kadanoff and G. Baym, *Quantum Statistical Mechanics: Green's Function Methods in Equilibrium and Non-Equilibrium Problems*, Advanced Book Classics (Perseus Books, 1989) ISBN 9780201094220

[21] J. Rammer and H. Smith, Rev. Mod. Phys. **58**, 323 (1986)

[22] S. Datta, J. Phys.: Condens. Matter **2**, 8023 (1990)

[23] J. Maassen, F. Zahid, and H. Guo, Phys. Rev. B **80**, 125423 (2009)

[24] M. Žnidarič and M. Horvat, Eur. Phys. J. B **86**, 1 (2013), ISSN 1434-6028

[25] N. Zimbovskaya and G. Gumbs, Appl. Phys. Lett. **81**, 1518 (2002)

[26] M. Zwolak and M. Di Ventra, Appl. Phys. Lett. **81**, 925 (2002)

[27] F. Gagel and K. Maschke, Phys. Rev. B **54**, 13885 (1996)

[28] D. Nozaki, Y. Girard, and K. Yoshizawa, J. Chem. Phys. C **112**, 17408 (2008)

[29] C. J. Cattena, R. Bustos-Marún, and H. M. Pastawski, Phys. Rev. B **82**, 144201 (2010)

[30] D. Nozaki, C. G. Rocha, H. M. Pastawski, and G. Cuniberti, Phys. Rev. B **85**, 155327 (2012)

[31] J. Qi, N. Edirisinghe, M. G. Rabbani, and M. P. Anantram, Phys. Rev. B **87**, 085404 (2013)

[32] W. Maryam, A. V. Akimov, R. P. Campion, and A. J. Kent, Nat. Commun. **4** (2013)

[33] A. Fert, Rev. Mod. Phys. **80**, 1517 (2008)

[34] H. M. Pastawski and E. Medina, Rev. Mex. Fis. **47S1**, 1 (2001)

[35] E. Domany, S. Alexander, D. Bensimon, and L. P. Kadanoff, Phys. Rev. B **28**, 3110 (1983)

[36] J. B. Sokoloff and J. V. José, Phys. Rev. Lett. **49**, 700 (1982)

[37] P. R. Levstein, H. M. Pastawski, and J. L. D'Amato, J. Phys.: Condens. Matter **2**, 1781 (1990)

[38] The infinitesimal η with the chosen sign ensures the correct branches of the solution. Note that this expression is easily obtained from the definition of the square root of a complex number:
$\sqrt{x + \mathrm{i}y} = \sqrt{\frac{r+x}{2}} + \mathrm{i}\,\mathrm{sgn}(y)\sqrt{\frac{r-x}{2}}$ where $r = |x + \mathrm{i}y|$.
Also note that the sign of this infinitesimal is consistent with Eq. 13.

[39] E. Rufeil Fiori and H. M. Pastawski, Chem. Phys. Lett. **420**, 35 (2006)

[40] I. Rotter, J. Phys. A: Math. Theor. **42**, 153001 (2009)

[41] A. D. Dente, R. A. Bustos-Marún, and H. M. Pastawski, Phys. Rev. A **78**, 062116 (2008)

[42] H. M. Pastawski, C. M. Slutzky, and J. F. Weisz, Phys. Rev. B **32**, 3642 (1985)

[43] W. H. Butler, Phys. Rev. B **8**, 4499 (1973)

[44] H. M. Pastawski, J. F. Weisz, and S. Albornoz, Phys. Rev. B **28**, 6896 (1983)

[45] L. E. F. Foa Torres, Phys. Rev. B **72**, 245339 (2005)

[46] V. Gasparian, T. Christen, and M. Büttiker, Phys. Rev. A **54**, 4022 (1996)

[47] R. Golizadeh-Mojarad and S. Datta, Phys. Rev. B **75**, 081301 (2007)

[48] B. C. Stipe, M. A. Rezaei, and W. Ho, Phys. Rev. Lett. **81**, 1263 (1998)

[49] H. Park, J. Park, A. K. L. Lim, E. H. Anderson, A. P. Alivisatos, and P. L. McEuen, Nature **407**, 57 (2000)

[50] J. Bonča and S. A. Trugman, Phys. Rev. Lett. **75**, 2566 (1995)

[51] J. Bonča and S. A. Trugman, Phys. Rev. Lett. **79**, 4874 (1997)

[52] C. A. Stafford and N. S. Wingreen, Phys. Rev. Lett. **76**, 1916 (1996)

[53] A. P. Jauho and N. S. Wingreen, Phys. Rev. B **58**, 9619 (1998)

[54] H. L. Calvo, H. M. Pastawski, S. Roche, and L. E. F. F. Torres, Appl. Phys. Lett. **98**, 232103 (2011)

[55] L. E. F. Foa Torres, H. M. Pastawski, and S. S. Makler, Phys. Rev. B **64**, 193304 (2001)

[56] R. P. Beardsley, A. V. Akimov, M. Henini, and A. J. Kent, Phys. Rev. Lett. **104**, 085501 (2010)

[57] H. M. Pastawski, L. E. F. Foa Torres, and E. Medina, Chem. Phys. **281**, 257 (2002)

[58] I. Camps, S. S. Makler, H. M. Pastawski, and L. E. F. Foa Torres, Phys. Rev. B **64**, 125311 (2001)

[59] E. V. Anda, S. S. Makler, H. M. Pastawski, and R. G. Barrera, Braz. J. Phys. **24**, 330 (1994)

[60] N. S. Wingreen, K. W. Jacobsen, and J. W. Wilkins, Phys. Rev. Lett. **61**, 1396 (1988)

[61] E. G. Emberly and G. Kirczenow, Phys. Rev. B **61**, 5740 (2000)

[62] C. J. Cattena, *Quantum decoherence effects on electronic transport in molecular wires and nanodevices*, Ph.D. thesis, Universidad Nacional de Córdoba (2012)

[63] T. Valet and A. Fert, Phys. Rev. B **48**, 7099 (1993)

[64] L. J. Fernández-Alcázar and H. M. Pastawski, Europhys. Lett. **105**, 17005 (2014)

[65] V. A. Gopar, D. Weinmann, R. A. Jalabert, and R. L. Stamps, Phys. Rev. B **69**, 014426 (2004)

[66] H. Saarikoski, T. Dollinger, and K. Richter, Phys. Rev. B **86**, 165407 (2012)